Chemistry, Physics and Technology of Surface. 2020. V. 11. N 4. P. 492-507

PACS numbers: 71.20.Nr; 72.80.Le; 72.80.Tm; 78.40.−q; 81.07.Wx; 81.15.Gh; 81.20.−n doi: 10.15407/hftp11.04.492

M.E. Bondarenko [1], P.M. Silenko [1], Yu.M. Solonin [1], A.V. Ragulya [1], M.M. Zahornyi [1], V.V. Shvalagin [2], N.I. Gubareni [1], O.Yu. Khyzhun [1]

INFLUENCE OF THE PHASE COMPOSITION OF THE TiO_2 MATRIX ON THE OPTICAL PROPERTIES AND MORPHOLOGY OF DEPOSITED $C_3N_4O_x$ NANOPARTICLES

[1] Frantsevich Institute for Problems of Materials Science of National Academy of Sciences of Ukraine
3 Krzhyzhanovsky Str., Kyiv, 03142, Ukraine, E-mail: mebondarenko@ukr.net
[2] Pisarzhevskii Institute of Physical Chemistry of National Academy of Sciences of Ukraine
31 Prospect Nauky, Kyiv, 03028, Ukraine

The use of oxygen modified graphite-like carbon nitride ($C_3N_4O_x$), photosensitive in the visible region of the optical spectrum, along with TiO_2, photocatalytically active only in the ultraviolet region of the spectrum, in the $C_3N_4O_x/TiO_2$ binary photocatalyst, opens a possibility of the use of sunlight energy. To increase opportunities of various kinds of photochemistry-related applications of $C_3N_4O_x/TiO_2$ photocatalyst, the phase composition of the TiO_2 matrix and morphology of nanoparticles of composite and their optical properties are very important. A novel composite material, $C_3N_4O_x/TiO_2$, was synthesized in the present work in accordance with the approach developed in Frantsevich Institute for Problems of Materials Science of NASU for the synthesis of powdered oxygen-doped carbon nitride ($C_3N_4O_x$) by CVD method under the special reactionary conditions of the melamine pyrolysis, in particular, in the presence of a fixed air volume. Deposition of $C_3N_4O_x$ carried out on the surface of a nanostructured powdered TiO_2 matrix of different phase composition, rutile or anatase. The deposition of $C_3N_4O_x$ (~5 % O) on both rutile and anatase nanopowders was confirmed by X-ray powder diffraction (XRD), scanning electron microscopy (SEM) with energy-dispersive X-ray spectroscopy (EDX), Fourier transform infrared spectroscopy (FTIR), X-ray photoelectron spectroscopy (XPS) and ultraviolet-visible diffuse reflectance spectroscopy (UV-Vis-DRS) methods. SEM micrographs (recorded with a MIRA3 TESCAN scanning electron microscope) of nanoparticles of both $C_3N_4O_x/TiO_2$ composites (anatase and rutile phases) demonstrate the arrangement of TiO_2 as separate globular nanoparticles and clusters between the plates and in the channels of the porous scaly plates $C_3N_4O_x$. However, the anatase phase nanoparticles (synthesized in IPM NASU) have a higher dispersion, the average size of non-aggregated almost monodisperse particles is about 10 nm. Using UV/Vis spectroscopy, it has been found that a redshift of long-wavelength edge of the fundamental absorption band of the spectra is observed when going from TiO_2 (anatase), TiO_2 (rutile), C_3N_4, $C_3N_4O_x/TiO_2$ (anatase), $C_3N_4O_x/TiO_2$ (rutile) and, then, to $C_3N_4O_x$, and the band gap decreases from 3.2, 3.0, 2.6, 2.4, 2.25 to 2.1 eV in the above sequence of materials. In such a case, $C_3N_4O_x/TiO_2$ (especially deposited on anatase phase) would absorb more visible light than g-C_3N_4 and TiO_2, by generating more charges which favor the improvement in the photoactivity of the catalysts.

***Keywords**: anatase, rutile, $C_3N_4O_x/TiO_2$ composite, O-doped carbon nitride, photocatalyst, pyrolysis, melamine*

INTRODUCTION

The environmental pollution and energy crisis become an increasing threat to the development of human society. Nowadays, the major challenge is to find new environmentally friendly ways to produce energy that may cover the global consumption, like the direct conversion of solar energy to an energy carrier (fuel, such as hydrogen obtained by photocatalytic water splitting), storable and usable upon request. The elaboration of new energy transforming systems using photocatalytic properties of TiO_2-based or carbon nitride (g-C_3N_4) systems is a promising way to the hydrogen synthesis by water photolysis, wastewater treatment and pathogenic microorganisms inactivation effectively, due to its superior photocatalytic oxidation performance and stable characteristics [1, 2]. Indeed, it is known that the use of unmodified TiO_2 as a photocatalyst is limited by a number of drawbacks, in particular, by the low quantum efficiency of the process due to the high rate of recombination of photogenerated electron-hole pairs, and the absorption spectrum limited by the ultraviolet region, which uses less than 7 % radiation from the sun for energy producing. Doping TiO_2 with various elements or

combination TiO_2 with another photocatalyst could open an opportunity to increase its activity [3–5].

In recent years graphite-like carbon nitride g-C_3N_4 has attracted broad interdisciplinary attention in solar energy conversion because of the excellent stability to photocorrosion and chemical corrosion, nontoxicity and low band gap being in the range 2.6–2.7 eV [6]. It is believed that the low electrical conduction of the pure g-C_3N_4 and the rapid photoelectron depletion cause an undesirable photon harvesting [6]. The authors of the review [6] highlighted that the variety of protocols involving heteroatom doping, morphology modification, hybrid copolymerization, exfoliation and co-catalysts had been employed to overcome these barriers and enhance the photocatalytic activity. The doping of carbon nitride by oxygen has been applied to extend the light absorption region of carbon nitride and, therefore, significantly improve its photocatalytic properties. It has been reported that O-g-C_3N_4 catalyst exhibits outstanding photocatalytic activity towards water splitting and organic pollutant degradation with simultaneous H_2 production under visible light [1, 7–12]. For example, use of ozone treated carbon nitride increases the rate constants of photocatalytic rhodamine B (RhB) degradation by *ca.* 6 times [10], accelerates the photodegradation of methylene blue (MB) by a factor of 5 and reveals twofold boost of the generation of H_2 compared with untreated graphitic carbon nitride [11]. The authors [8] reported the remarkable hydrogen evolution rate under catalysis by oxygen modified C_3N_4 sample compared with undoped g-C_3N_4, that was attributed to the synergy between extended visible light response, better separation of the photogenerated charge carriers and the enlarged specific surface area. It was assumed [12] that the significant enhancement of photocatalytic activity of O-doped carbon nitride could also be ascribed to the synergistic effects of narrowed band gap and improved charge transfer efficiency. Note that the most described methods of carbon nitride oxygen functionalization are multi-stage (at least two-stage). They involve post-synthesis treatment with ozone, nitric acid or hydrogen peroxide of pre-synthesized undoped g-C_3N_4 [11, 13–16]. For example, in [13], O-g-C_3N_4 was obtained by preliminary synthesis of non-oxygen contained g-C_3N_4 followed by prolonged (more than 10 h) treatment with hydrogen peroxide in a Teflon autoclave at 140 °C. At the Frantsevich Institute for Problems of Materials Science of NASU (IPM), a one-stage method of direct synthesis of oxygen-doped carbon nitride under special conditions of pyrolysis [17] of pyridine [18, 19], melamine [20], urea [21–23] or a mixture of cyanuric acid and urea [24] was proposed.

In the present work, we focus on a study of the photocatalytic TiO_2-based system associated with O-doped graphitic carbon nitride ($C_3N_4O_x$) [25], since the oxygen-modified graphitic carbon nitride samples synthesized in the IPM exhibit photosensitivity practically in the entire region of the visible spectrum. A number of publications are known to support the high photocatalytic activity of composites based on undoped g-C_3N_4 deposited on the surface rutile [26, 27], anatase [2, 3, 28–32] or comprises both anatase and rutile phases [33] TiO_2 matrix. For example, g-C_3N_4/TiO_2 (anatase phase) binary nanocomposite exhibits excellent bactericidal efficiency against *Escherichia coli* (*E. coli*) as a visible-light activated antibacterial coating [29]. The authors [29] attribute the bactericidal properties of the g-C_3N_4/TiO_2 composite to the formation of photo-promoted electrons that react with air oxygen to form superoxide radicals and related strong active oxidizers to deactivate bacteria cells under visible light. It is assumed that g-C_3N_4 acts as visible light absorber (sensitizer) that (based on relative energetic positions of the band) forms a junction with TiO_2 to facilitate electron hole separation, and, thus, suppresses recombination. In addition, the storage stability of g-C_3N_4/TiO_2 samples is very high: the samples keep ~99 and 94 % their bactericidal activity against *E. coli* after storage in dark and visible light at room temperature for 3 months, respectively. It was found [31] that the visible-light-induced photocatalytic degradation of methylene blue (MB) was remarkably increased upon formation of TiO_2/g-C_3N_4 couple and the best degradation performance of 70 % was obtained for 50 wt. % g-C_3N_4 loading. Based on the results obtained, the possible MB degradation mechanism is ascribed mainly to the generation of active species induced by the photogenerated electrons. The authors [27] report that the g-C_3N_4 (quantum dots) modified rutile TiO_2 (rTiO_2) hybrid (with nominal 15 at. % C_3N_4 loading) revealed the highest photocatalytic

activity among all the studied photocatalysts, used for degradation of toxic dye RhB or photocatalytic decomposition of NO, under visible light irradiation. Results described in [32] showed that the photocatalytic rate of Orange II (AO7) degradation under catalysis of the prepared g-C_3N_4/TiO_2 photocatalyst was about three times higher than that of pure TiO_2 and g-C_3N_4. It was suggested that the enhancement of photocatalytic activity can be attributed to the formation of heterojunctions between g-C_3N_4 and TiO_2, which leads to rapid charge transfer and the efficient separation of photogenerated electron-hole pairs. In the research [3], TiO_2 (anatase)/g-C_3N_4 nanocomposites were fabricated by three distinct synthetic protocols (co-calcination, solvothermal treatment and charge-induced aggregation), showing different degrees of (1.4–6.1 fold) of the visible-light induced photocatalytic hydrogen evolution reaction enhancement compared to the simple physical mixture. The authors [3] propose that the interfacial Ti–O–N covalent bonding promotes the charge carrier transfer and separation more effectively than the electrostatic interaction, thus accelerating the photocatalytic H_2 production. Meanwhile, the authors [3] attract attention to the fact that the exposed surface area of TiO_2 in the composite needs to be enlarged for the co-catalyst deposition. We think that it is essential for extension the possibilities of various types of photochemical applications of the $C_3N_4O_x$/TiO_2 photocatalyst, and it is important to study the effect of the phase composition of the TiO_2 matrix on the morphology of composite nanoparticles and their optical properties.

EXPERIMENTAL

Powdered $C_3N_4O_x$ (~ 5 % O) was obtained in accordance with the developed at Frantsevich Institute for Problems of Materials Science of the National Academy of Sciences of Ukraine (IPM NASU) facile one-step procedure for the synthesis of oxygen modified graphite-like carbon nitride at using various precursor [21–24] (melamine, in the present study) [20]. To produce a partially oxidized material, the melamine powder in the open ceramic crucible was placed in a tubular quartz reactor. For the present experiments, the synthesis of O-doped carbon nitride was carried out at heating a ceramic crucible up to 550 °C under ambient pressure. Pure $C_3N_4O_x$ and TiO_2, both rutile and anatase phases, were used for comparison. The deposition of oxygen-doped carbon nitride on a rutile or anatase nanostructured powdered matrix was carried out in accordance with the gas-phase method of direct synthesis of an individual $C_3N_4O_x$ powder under special reaction conditions for melamine pyrolysis [20, 25]. The peculiarity of the one-stage method (excluding the preliminary synthesis of oxygen-free g-C_3N_4 with its subsequent oxidation) for the preparation of oxygen-doped carbon nitride is that $C_3N_4O_x$ is formed in the presence of a fixed volume of air in the vapor-gas reaction space and is predominantly localized by means of deposition at lower temperatures (relative to the most high-temperature zone of localization of the precursor) zones of the quartz reactor. In order to obtain the nanostructured products $C_3N_4O_x$/TiO_2 (rutile phase) and $C_3N_4O_x$/TiO_2 (anatase phase), the studies were carried out by varying various technological (selection of the $C_3N_4O_x$ localization zone on anatase or rutile nanostructured powders) and reaction (temperature and heating time of the precursor in the highest temperature zone) parameters. Samples of pale yellow powders of $C_3N_4O_x$/TiO_2 composites (both rutile and anatase phases) were obtained by heat treatment of melamine at 520–580 °C for 0.5–1.5 h. Pure rutile and anatase powders and synthesized O-doped carbon nitride powder, $C_3N_4O_x$/TiO_2 (rutile phase) and $C_3N_4O_x$/TiO_2 (anatase phase) composites were denoted as TiO_2-R, TiO_2-A, $C_3N_4O_x$, $C_3N_4O_x$/TiO_2-R, $C_3N_4O_x$/TiO_2-A, respectively.

Synthesis of oxygen-doped carbon nitride ($C_3N_4O_x$) (~5 % O) on the surface of the nanostructured powdered TiO_2 matrix of different phase composition, rutile or anatase, is confirmed through various analytical techniques including X-ray powder diffraction (XRD), scanning electron microscopy (SEM) with energy-dispersive X-ray spectroscopy, Fourier transform infrared spectroscopy (FTIR), X-ray photoelectron spectroscopy (XPS) and ultraviolet-visible diffuse reflectance spectra (UV-Vis-DRS) methods.

The crystal structures were determined by powder X-ray diffraction (XRD) with a DRON-UM diffractometer using CuK_a radiation (λ = 1.54 Å) and a nickel filter. The powder X-ray diffraction measurements were carried out for 2θ in the range from 5 to 60 °.

The microstructure of the synthesized samples was verified by scanning electron microscopy (recorded with a MIRA3 TESCAN scanning electron microscope) equipped with an energy-dispersive X-ray spectrometer.

The surface compositions and elemental chemical states of the samples were examined using X-ray photoelectron spectroscopy (XPS) with a spectrometer manufactured by SPECS Surface Nano Analysis Company (Germany) equipped with a MgK_α X-ray source. The system is equipped with a PHOIBOS 150 hemispherical analyzer. The energy scale of the spectrometer was calibrated by setting the measured Au $4f_{7/2}$ and Cu $2p_{3/2}$ binding energies to 84.00±0.05 eV and 932.66±0.05 eV, respectively, with regard to E_F.

Fourier transform infrared spectroscopy (FTIR) in the reflectance mode was employed in the measuring range of 4000–400 cm^{-1} wavenumbers with the spectral resolution of 8 cm^{-1} using a Nexus Nicolet FTIR spectrometer (Thermo Scientific) equipped with a Smart Collector reflectance accessory. The samples were finely ground with KBr (in 1:100 ratio) for the transparent pellets.

Diffuse reflectance spectra (DRS) of the powders were recorded in the spectral range 200–1000 nm using a Perkin-Elmer Lambda Bio 35 UV-Vis with an integrating sphere Labsphere RSA-PR-20 with $BaSO_4$ as a scattering standard and converted into ultraviolet–visible (UV-Vis) absorption spectra by the Kubelka-Munk function [34]. The band gap energy was determined by plotting $(\alpha hv)^{1/2}$ vs photon energy.

RESULTS AND DISCUSSION

XRD analysis (Fig. 1) was performed to investigate the phase structure of the $C_3N_4O_x/TiO_2$-R and $C_3N_4O_x/TiO_2$-A composite samples, as well as the pure TiO_2 anatase (synthesized at the IPM NASU), TiO_2 rutile and O-modified carbon nitride $C_3N_4O_x$ samples.

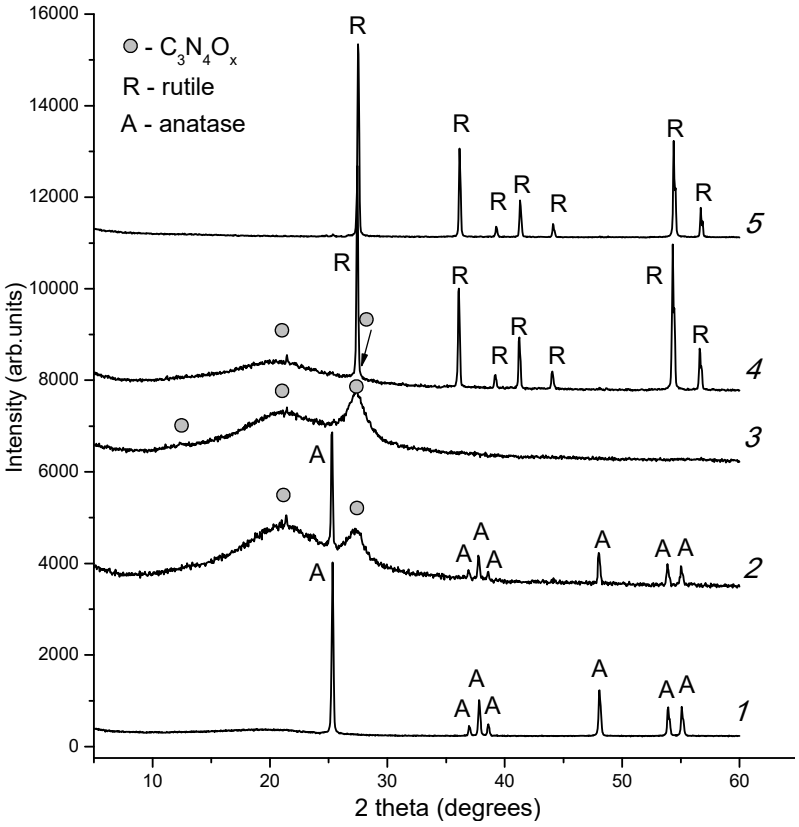

Fig. 1. XRD patterns of: *1* – pure TiO_2-A, *2* – $C_3N_4O_x/TiO_2$-A composite, *3* – pure $C_3N_4O_x$, *4* – $C_3N_4O_x/TiO_2$-R composite and *5* – pure TiO_2-R samples

In accordance with the one-stage method presented in the Experimental section, due to the heat treatment of melamine in the highest temperature reaction zone, for the ceramic crucible with TiO_2 powder placed in lower temperature zone, the pale yellow colored powder $C_3N_4O_x/TiO_2$ products are formed. With an increase in the synthesis temperature and the time of heat treatment, the color intensity of the obtained products increases. It should be noted that reflexes of residues of the precursor (melamine) are observed in the spectra of the samples obtained at 520–530 °C and heat treatment for 0.5 h. On XRD patterns of $C_3N_4O_x/TiO_2$-A (Fig. 1, curve *2*) and $C_3N_4O_x/TiO_2$-R (Fig. 1, curve *4*) composite samples, obtained at 565 °C for 1.5 h, the phase of precursor is not detected any more. As shown in Fig. 1, the XRD pattern of pure TiO_2-A as well as $C_3N_4O_x/TiO_2$-A composite evidence peaks at 25.4°, 37.0°, 37.9°, 38.7°, 48.3°, 54.1° and 55.4°, which correspond to (101), (103), (004), (112), (200), (105) and (211) planes of the crystal facet of anatase TiO_2 (JCPDS No. 21-1272), respectively. Similarly, there are strong peaks characteristic for the rutile phase (JCPDS No. 21-1276) with the most intense reflexes at $2\theta = 27.4°$ (110), 36.2° (101) and 54.4° (211) on the XRD pattern of the $C_3N_4O_x/TiO_2$-R composite and pure TiO_2-R samples.

There are known two typical diffraction peaks at approximately $2\theta = 12.40°$ and 27.49° in XRD patterns of undoped graphitic carbon nitride, corresponding to the (100) and (002) planes of g-C_3N_4, which are attributed to the in-plane structure of tri-*s*-triazine units and the interlayer stacking of conjugated aromatic groups, respectively (JCPDS 87-1526). The reflex at $2\theta = 27.49$ ° characterizes the distance (~0.324 nm) between adjacent nitride-carbon monolayers. Broadening and decreasing the intensity of this peak on the X-ray diffraction pattern of $C_3N_4O_x$ (Fig. 1, curve *3*) is associated with disordering of the layered structure of oxygen-doped carbon nitride due to the presence of oxygen-containing functional groups [20, 24, 25]. In addition, the extremely weak peak at 12.40° almost invisible on XRD pattern in the O-modified sample ($C_3N_4O_x$) indicates the dearomatization of some triazine units in such a case [8]. The appearance of an additional reflex at $2\theta = 21.45$ ° ($d = 0.414$ nm) on the X-ray diffraction pattern of O-doped carbon nitride is caused, as suggested in [8, 20, 24], with partial distortion of the planarity of its polymer network $((C_6N_7)–N)_n$. This is due to the oxidation of g-C_3N_4, which may give rise to the dearomatization of some heterocycles (–C=N– to –C(OH)–NH–). The dearomatized heterocycles can also deform the planarity of a heptazine plane and promote the formation of an additional much bigger interplanar distance [8, 20, 24]. To confirm the obtaining of binary composites, it is important to note that on the XRD patterns of both products $C_3N_4O_x/TiO_2$-A (Fig. 1, curve *2*) and $C_3N_4O_x/TiO_2$-R (Fig. 1, curve *4*), the broadened low-intensity peak at 27.49° as well as a wide halo at 21.45° (which is characteristic for O-doped carbon nitride) are also clearly observed. However, for $C_3N_4O_x/TiO_2$-R composite sample (Fig. 1, curve *4*), one typical peak of $C_3N_4O_x$ (002) is less clearly observed due to its coverage by rutile TiO_2 (110). With the use of FT-IR, g-$C_3N_4O_x/TiO_2$ composite was more easily identified.

Fourier-transform infrared spectroscopy (FT-IR) spectra of the experimental samples ($C_3N_4O_x$, $C_3N_4O_x/TiO_2$-A and $C_3N_4O_x/TiO_2$-R) shown in Fig. 2 clearly confirm the formation of $C_3N_4O_x$ on the surface of TiO_2 marix. FT-IR spectra of pure melamine precursor and both TiO_2 rutile and anatase matrix were used for comparison. The characteristic signals for $C_3N_4O_x$ could be observed in the spectra of all synthesized samples (Fig. 2, curves *2*, *3*, *4*) indicating that the intact triazine structure remains in the product after the deposition on the surface of nanostructured TiO_2 matrix. The peaks at 810 cm^{-1} and in the 1200–1650 cm^{-1} region are assigned to the out-of-plane bending vibrations of triazine ring in the tri-*s*-triazine (heptazine) units in $C_3N_4O_x$ and the stretching vibrations of aromatic CN bonds in condensed carbon-nitrogen heterocycles, respectively. It is quite logical that peak near 810 cm^{-1} characteristic for triazine ring is also observed in the spectrum of the melamine precursor (Fig. 2, curve *1*). Weak line at 2148 cm^{-1} associated with triple-bond cyano groups in the synthesized material is usually attributed to incomplete polymerization of the precursor. A more detailed characterization of carbon nitride absorption bands in the 1200–1650 cm^{-1} region is presented in the study [35]. The authors [35] suggest that the bands near 1650–1600 cm^{-1} correspond to double C=N bond stretching modes, whereas the

band near 1500 cm^{-1} is formed by a double ring quadrant stretch mode. The group of absorption lines near 1400–1450 cm^{-1} presents tri-*s*-triazine aromatic rings double bond C=N stretching modes. The peaks in the 1200–1350 cm^{-1} region can be related to the C–N bonds stretching, in particular, the strong band observed near 1320 cm^{-1} characterizes the C–N stretch in the threefold N-bridge linking the tri-*s*-triazine rings [35].

Along with the signals typical for the carbon nitride network, weak signals characteristic only for oxidized carbon nitride and the oxygen-containing functional groups (–OH, >C=O and –COOH), are detected in the spectra of all three synthesized samples. The weak peak near 1080 cm^{-1} is attributed to the stretching C–O vibration, while the N–H and O–H bands around 3000–3600 cm^{-1} are generally related to hydroxyl groups. Weak signal in the spectra of composite samples becomes to emerge at ~1750 cm^{-1} that suggests the formation of carbonyl (carboxyl) groups. The presence of carboxyl groups is an evidence of a stretching band at ~2700 cm^{-1}, characteristic for –O–H bond of carboxyl group. Note that, the presence of oxygen-containing functional groups confirms that oxygen is doped into the $C_3N_4O_x$ lattice being in a good agreement with literature [13, 14, 33, 35–37]. However, as we noted earlier in [25], oxygen position in O-modified carbon nitride network is currently still under discussion. Probably in the structure of the $C_3N_4O_x$ lattice, both the addition of oxygen in the form of functional groups and the substitution of two-coordinated nitrogen with oxygen are possible.

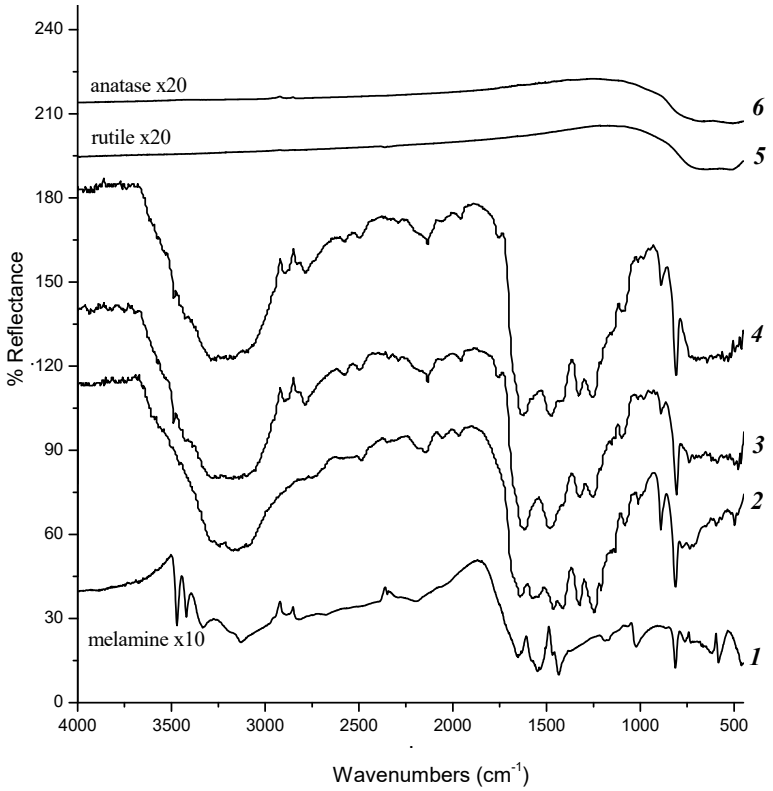

Fig. 2. IR spectra: *1* – melamine precursor, *2* – pure $C_3N_4O_x$, *3* – $C_3N_4O_x/TiO_2$-R composite, *4* – $C_3N_4O_x/TiO_2$-A composite, *5* – pure TiO_2-R and *6* – pure TiO_2-A samples

Pure TiO_2 (Fig. 2, curves *5, 6*) shows characteristic broad absorption band in the FT-IR spectra at 450–800 cm^{-1}. As shown in Fig. 2, the broad absorption band observed below 800 cm^{-1} for neat TiO_2 could be attributed to Ti–O–Ti and Ti–O stretching vibration modes in both rutile and anatase crystals [32, 33]. For the $C_3N_4O_x/TiO_2$ samples, despite the strong light scattering of TiO_2 at low wavenumbers as well as the fact that the surface of the particles of anatase or rutile powders,

probably, is almost completely covered with O-doped carbon nitride, weak wide signals near 800 cm^{-1} were observed (Fig. 2, curves *3, 4*). In addition, as can be seen from Fig. 2, the FT-IR spectra of pure $C_3N_4O_x$ and $C_3N_4O_x/TiO_2$ composites show no much noticeable differences. However, compared to pure $C_3N_4O_x$, the FT-IR spectra of both composites ($C_3N_4O_x/TiO_2$-A and $C_3N_4O_x/TiO_2$-R) are weakly structured. This can be associated with an increase in the degree of disordering the structure of both samples based on the $C_3N_4O_x/TiO_2$ composite.

Morphologies and microstructures of the nanocomposites, pure O-doped carbon nitride, pure rutile and anatase matrices were studied by SEM technique. The results are shown in Figs. 3 and 4. As seen from Fig. 3 *a*, pure $C_3N_4O_x$ reveals the lamellar stacking structure typical for undoped g-C_3N_4 consisting of thin, continuous, and wrinkleenriched nanosheets [32]. In general, the O-doped carbon nitride material consists of multiple layers of plane sheets covered with small flat flakes and particles of different sizes being in the range from several micrometers to 20 nm [35]. As shown in Fig. 3 *b*, *c* neat TiO_2-A as well as TiO_2-R comprised irregular aggregates of particles.

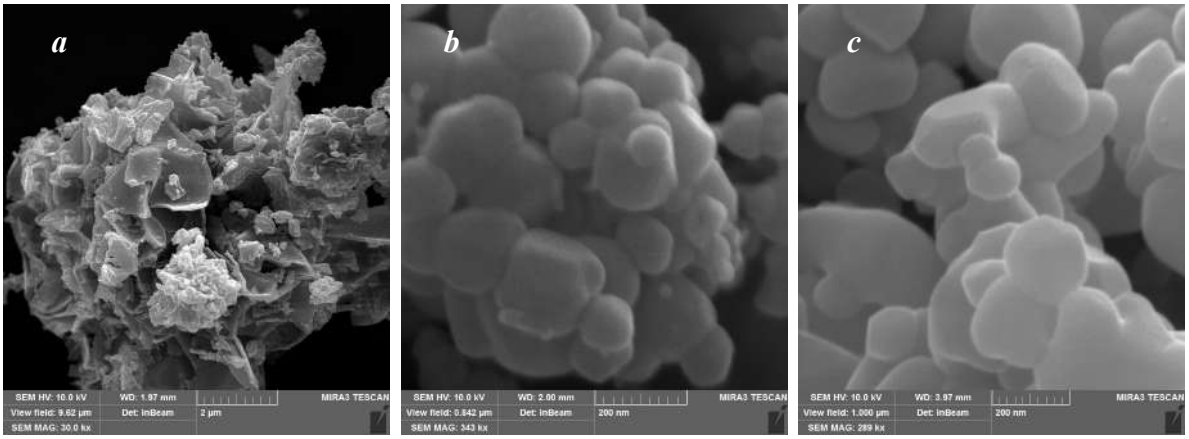

Fig. 3. SEM microphotographs of the powders: pure $C_3N_4O_x$ (*a*), TiO_2-A (*b*), TiO_2-R (*c*)

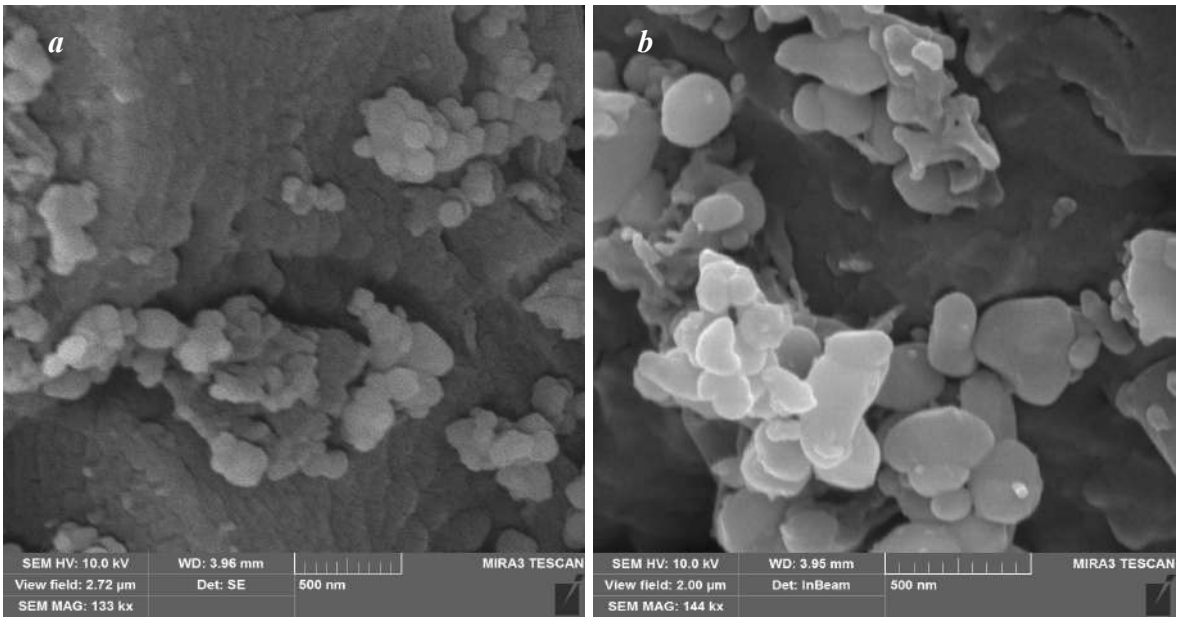

Fig. 4. SEM images of composites $C_3N_4O_x/TiO_2$-A (*a*) and $C_3N_4O_x/TiO_2$-R (*b*)

SEM micrographs (Fig. 4) of nanoparticles of both $C_3N_4O_x/TiO_2$ composites (anatase and rutile phase) demonstrate the arrangement of TiO_2 as separate globular nanoparticles and clusters between the plates and in the channels of porous $C_3N_4O_x$ plates. However, the anatase phase nanoparticles have a significantly higher dispersion, the average size of non-aggregated almost monodisperse particles is about 10–20 nm (a detailed study of the characteristics of synthesized at the IPM of NASU anatase nanoparticles is presented in [38]). High-resolution SEM showed that the TiO_2 matrix of the anatase (Fig. 3 *a*) and rutile phase (Fig. 3 *b*) consists of soft aggregates with sizes ranging from 100 to 200 nm and from 100 to 300 nm, respectively. Moreover, TiO_2-A nanoparticles are found to be completely embedded in the carbon nitride lamellar structure and are well dispersed on $C_3N_4O_x$ (Fig. 4 *a*), indicating that the presence of $C_3N_4O_x$ suppressed the aggregation of TiO_2 anatase nanoparticles.

Energy dispersive X-ray spectroscopy (EDX) was used to investigate the composition of $C_3N_4O_x/TiO_2$ samples. As shown in Fig. 5, in particular, the composition of $C_3N_4O_x/TiO_2$-R composite estimated with EDX analysis is represented by only four main elements: carbon, nitrogen, oxygen and titanium. It should be noted that, according to EDX results, an increase in the oxygen content in the composite is accompanied by a decrease in the nitrogen content. This can indirectly indicate on the substitution of two-coordinated nitrogen with oxygen in the structure of $C_3N_4O_x$ lattice. These results confirm the successful synthesis of O-doped carbon nitride and loading $C_3N_4O_x$ on TiO_2 matrix.

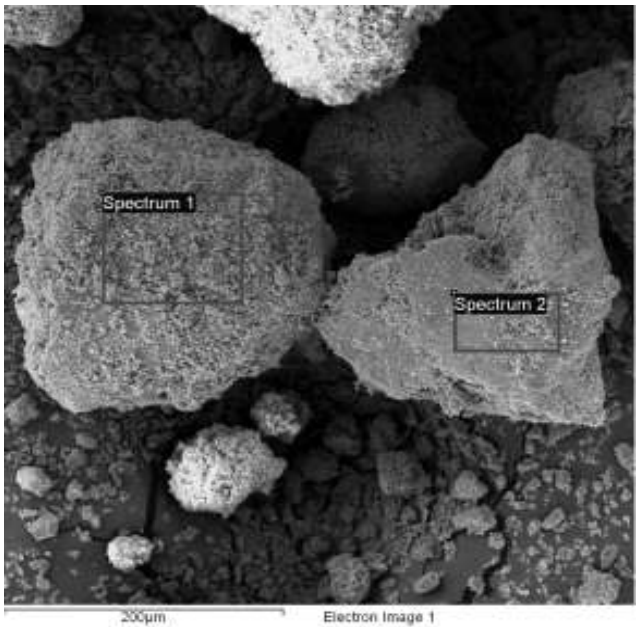

Processing option : All elements analysed (Normalised)

Spectrum	In stats.	C	N	O	Ti	Total
Spectrum 1	Yes	39.79	46.02	7.98	6.21	100.00
Spectrum 2	Yes	39.62	44.25	11.20	4.93	100.00
Mean		39.71	45.13	9.59	5.57	100.00
Std. deviation		0.12	1.25	2.27	0.90	
Max.		39.79	46.02	11.20	6.21	
Min.		39.62	44.25	7.98	4.93	

All results in weight%

Fig. 5. SEM image and the composition of the material estimated with the EDX spectroscopy of $C_3N_4O_x/TiO_2$-R composite

XPS was utilized to investigate the oxidation state and surface chemical compositions of the $C_3N_4O_x/TiO_2$-R and $C_3N_4O_x/TiO_2$-A nanocomposites. As shown in Fig. 6, the core-level spectra associated with C, N, O, and Ti are detected in the survey XPS spectra of both composites. No peaks of other elements were found revealing that the $C_3N_4O_x/TiO_2$-R and $C_3N_4O_x/TiO_2$-A heterojunction photocatalysts are mainly composed of C, N, O, and Ti elements; this consequence is in agreement with the result of EDX (Fig. 5). The XPS results presented in Fig. 6 show that the spectra of the two composites reveal no significant differences.

The high resolution XPS spectra of N 1*s* electrons of both composites are shown in Fig. 7 *a*. The deconvolution of the N1*s* spectrum (Fig. 7 *b*) of the $C_3N_4O_x/TiO_2$-R composite yields the presence of two main peaks centered at 398.5 and 399.8 eV that can be attributed to N atoms corresponding to sp^2-hybridized nitrogen (C=N–C) and sp^3-hybridized nitrogen (N–$(C)_3$) atoms in the carbon nitride network, respectively.

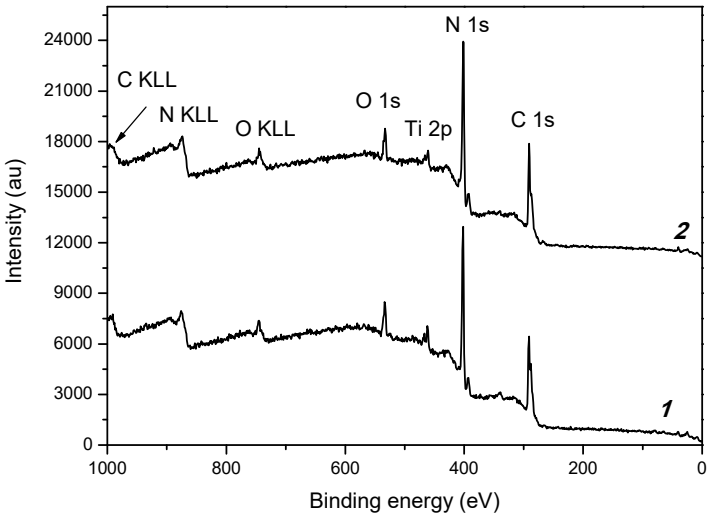

Fig. 6. Survey XPS spectra: *1* – $C_3N_4O_x/TiO_2$-A composite and *2* – $C_3N_4O_x/TiO_2$-R composite

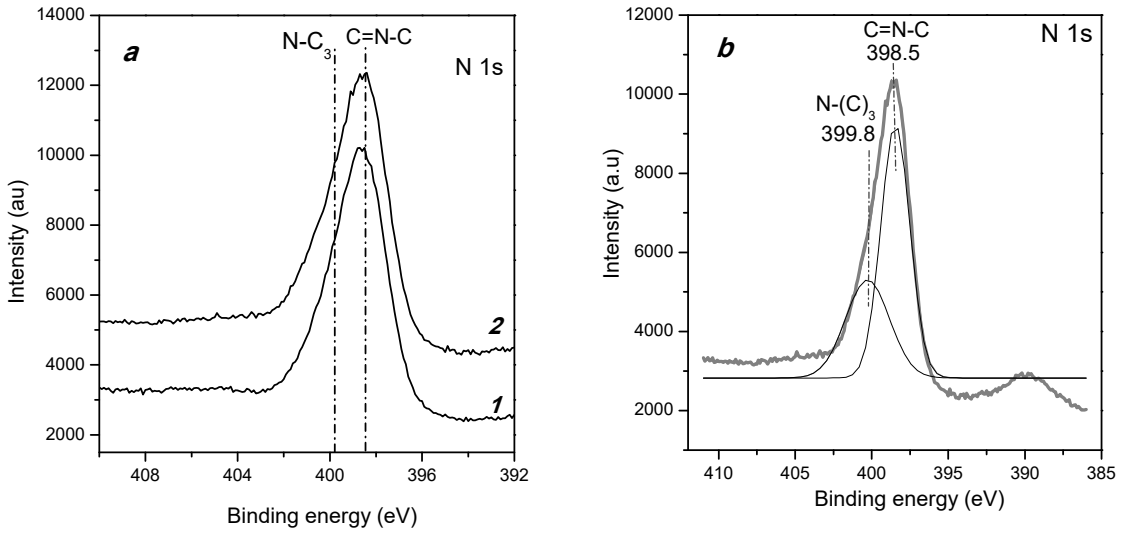

Fig. 7. N 1*s* XPS spectra (*a*) of *1* – $C_3N_4O_x/TiO_2$-A composite and *2* – $C_3N_4O_x/TiO_2$-R composite; the deconvolution of N 1*s* XPS spectrum (*b*) of $C_3N_4O_x/TiO_2$-R sample

The XPS C 1*s* core-level spectra of the $C_3N_4O_x/TiO_2$-R and $C_3N_4O_x/TiO_2$-A samples are presented in Fig. 8 *a*. The spectra can be deconvoluted into three peaks, the most intensive peak at 288.0 eV is indicative of the sp^2-hybridized C (N=C–N bond) in the triazine unit. The weaker C 1*s* peak at 284.6 eV corresponds to the C–C coordination and it is always presented in the spectra of carbon nitride that could be explained by hydrocarbon adsorption on the sample surfaces due to their contact with laboratory air prior to the XPS measurements started being in a good agreement with literature [6, 11, 13, 14]. The third weak peak is observed at ~290 eV as a result of the incorporation of C=O or C–O groups (as seen in Figs. 8, 9) on the surface of the O-doped carbon nitride materials [11, 13, 14], which is in agreement with the FT-IR results.

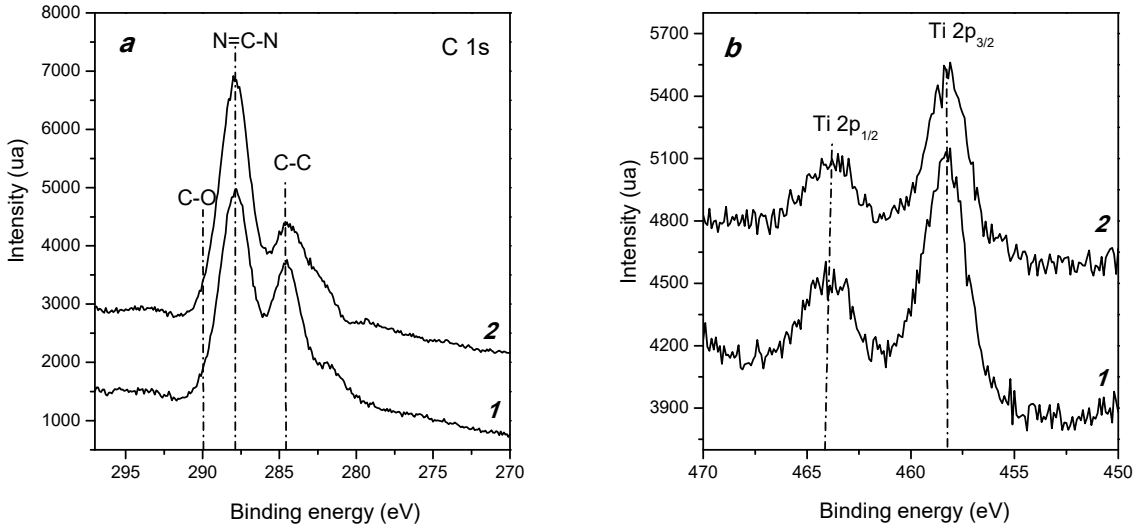

Fig. 8. C 1*s* (*a*) and Ti 2*p* (*b*) XPS spectra: *1* – $C_3N_4O_x/TiO_2$-A composite and *2* – $C_3N_4O_x/TiO_2$-R composite

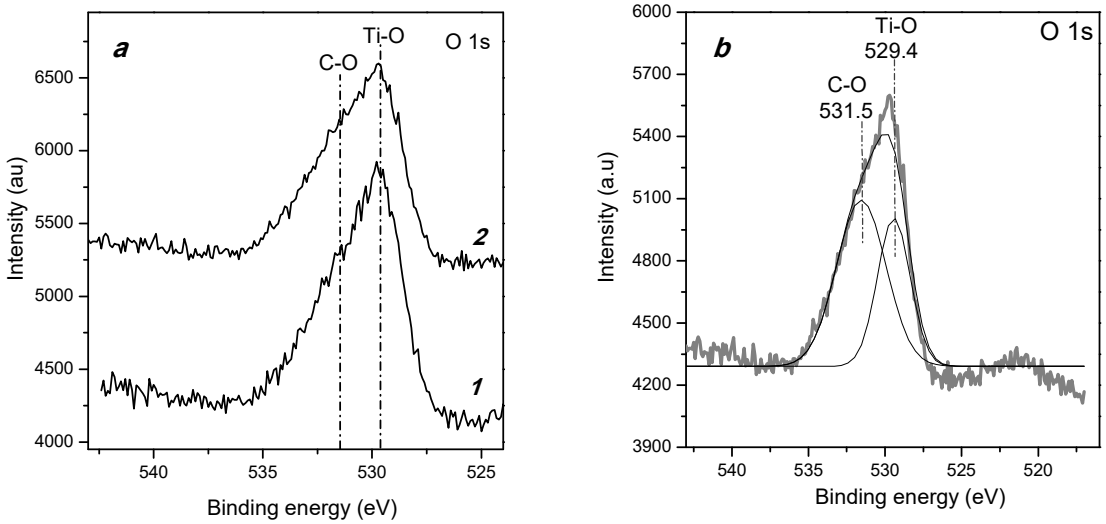

Fig. 9. O 1*s* XPS spectra (*a*): *1* – $C_3N_4O_x/TiO_2$-A composite and *2* – $C_3N_4O_x/TiO_2$-R composite; the deconvolution of O 1*s* XPS spectrum (*b*) of $C_3N_4O_x/TiO_2$-R sample

As illustrated in Fig. 8 *b*, the Ti 2*p* spectra of both $C_3N_4O_x/TiO_2$ composites have two peaks at 458.2 and 464.1 eV, corresponding to Ti2$p_{3/2}$ and Ti2$p_{1/2}$ of TiO_2, respectively. It is important to note that, according to XPS, the content of Ti on the surface of both composites is no more than 4 wt. %, this result is in a good agreement with the data by EDX. Hence, the surface of the particles of both TiO_2 matrices is almost completely covered with O-modified carbon nitride. This fact explains the weak intensity of the Ti 2*p* peaks on the survey XPS spectra.

In Fig. 9 *a*, *b*, the XPS O 1s spectrum presents two characteristic peaks located at 531.2 and 529.4 eV corresponding to C–O bond in the O-doped carbon nitride [13, 20, 24, 25] and Ti–O bond in titanium dioxide, respectively. According to the XPS results, on the surface of the samples of both composites, the oxygen content in $C_3N_4O_x$ (O-C bond) is higher than the oxygen content in the TiO_2 matrix (O-Ti bond). For example, for $C_3N_4O_x/TiO_2$-R sample, total 7.6 wt. % O is in satisfactory agreement with the EDX results, while the oxygen contents in $C_3N_4O_x$ and TiO_2 are 4.9 and 2.7 wt. %, respectively. These observations, together with the SEM results, suggest the formation of heterojunction between TiO_2 and $C_3N_4O_x$ that would be a successful system (especially $C_3N_4O_x/TiO_2$-A) to achieve the improved electron-hole separation.

Surface modification would have a significant impact on the light response properties of the samples, characterized by UV-Vis diffuse reflectance spectroscopy. Fig. 10 presents that the optical absorption capabilities of undoped g-C_3N_4, rutile, anatase, synthesized O-modified $C_3N_4O_x$ samples, $C_3N_4O_x/TiO_2$-R and $C_3N_4O_x/TiO_2$-A composite samples were analyzed using UV–Vis absorption spectroscopy. The optical absorption spectra reveal that the pure anatase and rutile phase TiO_2 samples feature an intrinsic semiconductor-like absorption in the ultraviolet region (with the edge of the absorption band near 380 and 410 nm, respectively) as evidenced from Fig. 10 (curves *1*, *2*). Accordingly, both TiO_2 samples reveal large band gaps characteristic for titanium dioxide, in particular ~ 3.2 and ~3.0 eV for anatase and rutile, respectively (Fig. 11, curves *1*, *2*).

The undoped g-C_3N_4 sample shows a typical feature of a photosensitive semiconductor possessing an intrinsic characteristic absorption peak with long-wavelength edge of the fundamental absorption band at ~460 nm (Fig. 10, curve *6*), corresponding to the band gap energy of 2.6 eV for photoexcited electron, as shown in Fig. 11 (curve *6*). Such a feature is attributed to the lone pair of electrons of nitrogen atom in valance band jumping into the π bonding electronic conduction band.

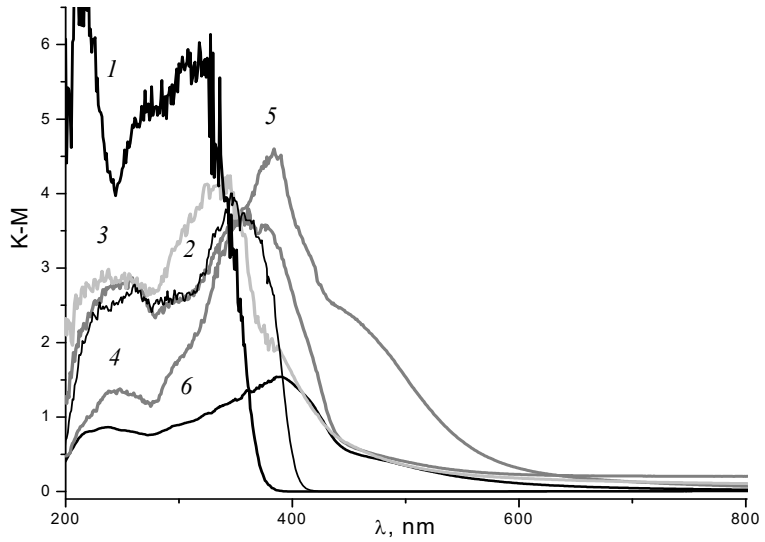

Fig. 10. UV-Vis diffuse reflectance spectra converted by the Kubelka-Munk function: *1* – pure TiO_2-A, *2* – pure TiO_2-R, *3* – $C_3N_4O_x/TiO_2$-A composite, *4* – $C_3N_4O_x/TiO_2$-R composite, *5* – pure $C_3N_4O_x$ and *6* – undoped C_3N_4 samples

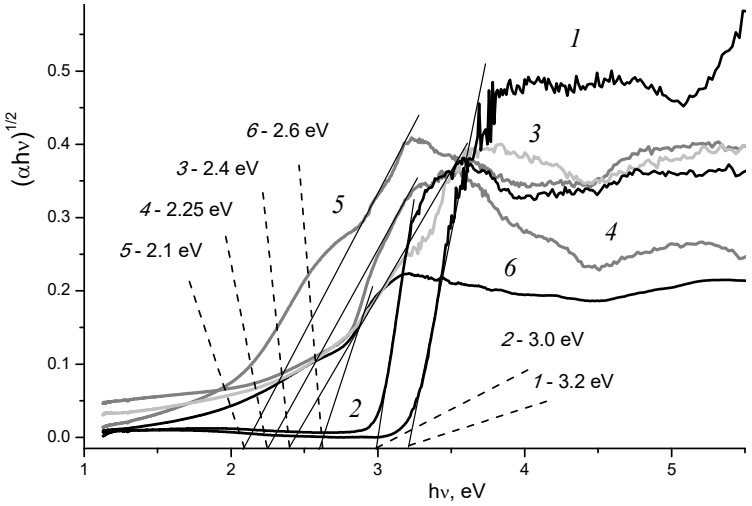

Fig. 11. Estimation of band gap energies E_g: *1* – pure TiO_2-A, *2* – pure TiO_2-R, *3* – $C_3N_4O_x/TiO_2$-A composite, *4* – $C_3N_4O_x/TiO_2$-R composite, *5* – pure $C_3N_4O_x$ and *6* – undoped C_3N_4 samples

There is a bathochromic shift of the absorption edge which expands to the significant part of the visible light region for all synthesized powders ($C_3N_4O_x$, $C_3N_4O_x/TiO_2$-R and $C_3N_4O_x/TiO_2$-A) doped with oxygen (from 460 nm for undoped g-C_3N_4 to 600 nm with absorption trailing extended to more than 700 nm for $C_3N_4O_x$) (Fig. 10, curves *3*, *4*, *5*). It is assumed that, in comparison with undoped g-C_3N_4, the absorption band edge of $C_3N_4O_x$ is red shifted due to the presence of O-doping, possibly due to excitation into the lower energy defect states [39, 40]. It was found [37] that the red shift in the absorption wavelength indicates that the introduction of oxygen results in the higher absorption of light energy to produce more photogenerated electron-hole pairs, which contribute to the improvement in the photoactivity of the catalysts.

The absorption band edges of $C_3N_4O_x/TiO_2$-R and $C_3N_4O_x/TiO_2$-A composites are located between those of both pure TiO_2 samples and oxygen modified $C_3N_4O_x$ samples that additionally confirm the electronic coupling of these two components in the $C_3N_4O_x/TiO_2$ heterojunction. In summary, it has been found that in the series from TiO_2-A, TiO_2-R, C_3N_4, $C_3N_4O_x/TiO_2$-A, $C_3N_4O_x/TiO_2$-R to $C_3N_4O_x$, a redshift of long-wavelength edge of the fundamental absorption band is observed in the spectra (Fig. 10), and the band gap (Fig. 11) decreases from 3.2, 3.0, 2.6, 2.4, 2.25 to 2.1 eV respectively. In such a case, $C_3N_4O_x/TiO_2$ composite would absorb more visible light than both TiO_2 and undoped g-C_3N_4 samples by generating more charges; this should contribute to the improvement in the photoactivity of the catalysts.

CONCLUSIONS

The above results demonstrate that the $C_3N_4O_x/TiO_2$-R and $C_3N_4O_x/TiO_2$-A heterojunction photocatalysts were successfully synthesized. As a result of our studies, we have demonstrated that the phase modification of the TiO_2 matrix does not affect significantly the chemical composition of both synthesized materials. Both composites are capable to absorb light in the visible range of the optical spectrum and the band gaps of $C_3N_4O_x/TiO_2$-A and $C_3N_4O_x/TiO_2$-R are 2.4 and 2.25 eV, respectively. The synthesized materials reveal improved photosensitivity for the obtained composites due to the absorption of a wider spectrum of light energy in comparison with individual samples of titanium dioxide and undoped g-C_3N_4, as well as the possibility of spatial separation of photogenerated charges between the components of the composite, which reduces the negative effect of electron-hole recombination.

ACKNOWLEDGEMENTS

This work was partially supported by research project of National Academy of Sciences of Ukraine “Development of innovative photocatalytic nanostructured materials based on ZnO and TiO_2” (528/IPM-11/20).

Вплив фазового складу матриці TiO_2 на оптичні властивості та морфологію осаджених наночастинок $C_3N_4O_x$

М.Е. Бондаренко, П.М. Силенко, Ю.М. Солонін, А.В. Рагуля, М.М. Загорний, В.В. Швалагін, Н.І. Губарені, О.Ю. Хижун

Інститут проблем матеріалознавства ім. І.М. Францевича Національної академії наук України
вул. Кржижановського, 3, Київ, 03142, Україна, mebondarenko@ukr.net
Інститут фізичної хімії ім. Л.В. Писаржевського Національної академії наук України
просп. Науки, 31, Київ, 03028, Україна

Використання модифікованого киснем графітоподібного нітриду вуглецю ($C_3N_4O_x$), фоточутливого у видимій області спектра, поряд з TiO_2, який виявляє фотокаталітичну активність тільки під дією УФ опромінювання, в складі бінарного фотокаталізатора $C_3N_4O_x/TiO_2$, дозволяє використовувати енергію сонячного світла. Для розширення можливостей різних видів фотохімічного застосування фотокаталізаторів $C_3N_4O_x/TiO_2$ важливе значення мають фазовий склад матриці TiO_2, морфологія наночастинок композиту і їхні оптичні властивості. Композитний матеріал - $C_3N_4O_x/TiO_2$ був синтезований відповідно з підходом, розробленим в Інституті проблем матеріалознавства ім. І.М. Францевича НАН України для синтезу порошку легованого киснем нітриду вуглецю ($C_3N_4O_x$) методом CVD в особливих реакційних умовах (в присутності фіксованого обсягу повітря) піролізу меламіну. Осадження $C_3N_4O_x$ проводять на поверхню наноструктурованої порошкоподібної матриці TiO_2 різного фазового складу - рутилу або анатазу. Осадження $C_3N_4O_x$ (~5 % O) на поверхні нанопорошків як рутилу, так і анатазу, підтверджено методами рентгенівської порошкової дифракції, скануючої електронної мікроскопії з методом енергодисперсійної рентгенівської спектроскопії, інфрачервоної спектроскопії з Фур'є-перетворенням, рентгенівської фотоелектронної спектроскопії та спектрами дифузного відбиття в ультрафіолетовому та видимому діапазоні. СЕМ-мікрофотографії (визначали на скануючому електронному мікроскопі MIRA3 TESCAN) наночастинок обох композитів $C_3N_4O_x/TiO_2$ (анатазної і рутилової фази) демонструють розташування TiO_2 у вигляді окремих глобулярних наночастинок і кластерів між пластинами і в каналах пористих лускатих пластин $C_3N_4O_x$. Однак наночастинки фази анатазу (синтезованого в ІПМ НАНУ) мають вищу дисперсність, середній розмір неагрегованих майже монодисперсних частинок становить 10 нм. Дослідження спектрів поглинання зразків показало, що в ряду від TiO_2 (анатаз), TiO_2 (рутил), C_3N_4, $C_3N_4O_x/TiO_2$ (анатаз), $C_3N_4O_x/TiO_2$ (рутил) до $C_3N_4O_x$, спостерігається червоне зміщення довгохвильового краю основної смуги поглинання в спектрах, ширина забороненої зони зменшується з 3.2, 3.0, 2.6, 2.4, 2.25 до 2.1 еВ відповідно. В такому випадку $C_3N_4O_x/TiO_2$ (особливо осаджений на фазі анатазу) буде поглинати більше видимого світла, ніж та g-C_3N_4, і TiO_2, створюючи при цьому більше зарядів, що сприяє поліпшенню фотоактивності каталізаторів.

***Ключові слова**: анатаз, рутил, композит $C_3N_4O_x/TiO_2$, О-допований нітрид вуглецю, фотокаталізатор, піроліз, меламін*

Влияние фазового состава матрицы TiO_2 на оптические свойства и морфологию осажденных наночастиц $C_3N_4O_x$

М.Э. Бондаренко, П.М. Силенко, Ю.М. Солонин, А.В. Рагуля, М.Н. Загорный, В.В. Швалагин, Н.И. Губарени, О.Ю. Хижун

Институт проблем материаловедения им. И.М. Францевича Национальной академии наук Украины
ул. Кржижановского, 3, Киев, 03142, Украина, mebondarenko@ukr.net
Институт физической химии им. Л.В. Писаржевского Национальной академии наук Украины
просп. Науки, 31, Киев, 03028, Украина

Использование модифицированного кислородом графитоподобного нитрида углерода ($C_3N_4O_x$), фоточувствительного в видимой области спектра, наряду с TiO_2, который проявляет

фотокаталитическую активность только под действием УФ облучения, в составе бинарного фотокатализатора $C_3N_4O_x/TiO_2$, позволяет использовать энергию солнечного света. Для расширения возможностей различных видов фотохимического применения фотокатализаторов $C_3N_4O_x/TiO_2$ важное значение имеют фазовый состав матрицы TiO_2, морфология наночастиц композита и их оптические свойства. Композитный материал - $C_3N_4O_x/TiO_2$ был синтезирован в соответствии с подходом, разработанным в Институте проблем материаловедения им. И.Н. Францевича НАН Украины для синтеза порошка легированного кислородом нитрида углерода ($C_3N_4O_x$) методом CVD в особых реакционных условиях (в присутствии фиксированного объема воздуха) пиролиза меламина. Осаждение $C_3N_4O_x$ проводят на поверхность наноструктурированной порошкообразной матрицы TiO_2 различного фазового состава - рутила или анатаза. Осаждение $C_3N_4O_x$ (~5 % O) на поверхности нанопорошков как рутила, так и анатаза, подтверждено методами рентгеновской порошковой дифракции, сканирующей электронной микроскопии с энергодисперсионной рентгеновской спектроскопией, инфракрасной спектроскопии с Фурье-преобразованием, рентгеновской фотоэлектронной спектроскопии и спектрами диффузного отражения в ультрафиолетовом и видимом диапазоне. СЭМ-микрофотографии (определяли на сканирующем электронном микроскопе MIRA3 TESCAN) наночастиц обоих композитов $C_3N_4O_x/TiO_2$ (анатазной и рутиловой фазы) демонстрируют расположение TiO_2 в виде отдельных глобулярных наночастиц и кластеров между пластинами и в каналах пористых чешуйчатых пластин $C_3N_4O_x$. Однако наночастицы фазы анатаза (синтезированного в ИПМ НАНУ) имеют более высокую дисперсность, средний размер неагрегированных почти монодисперсных частиц составляет 10 нм. Исследование спектров поглощения образцов показало, что в ряду от TiO_2 (анатаз), TiO_2 (рутил), C_3N_4, $C_3N_4O_x/TiO_2$ (анатаз), $C_3N_4O_x/TiO_2$ (рутил) до $C_3N_4O_x$, наблюдается красное смещение длинноволнового края основной полосы поглощения в спектрах, ширина запрещенной зоны уменьшается с 3.2, 3.0, 2.6, 2.4, 2.25 до 2.1 эВ соответственно. В таком случае $C_3N_4O_x/TiO_2$ (особенно осажденный на фазе анатаза) будет поглощать больше видимого света, чем g-C_3N_4, и TiO_2, создавая при этом больше зарядов, что способствует улучшению фотоактивности катализаторов.

***Ключевые слова**: анатаз, рутил, композит $C_3N_4O_x/TiO_2$, O-допированный нитрид углерода, фотокатализатор, пиролиз, меламин*

REFERENCES

1. Putri L.K., Ng B.J., Er C.C., Ong W.J., Chang W.S., Mohamed A.R., Chaia S.P. Insights on the impact of doping levels in oxygen-doped gC_3N_4 and its effects on photocatalytic activity. *Appl. Surf. Sci*. 2020. **504**: 144427.
2. Lei J., Chen B., Lv W., Zhou L., Wang L., Liu Y., Zhang J. Inverse opal TiO_2/g-C_3N_4 composite with heterojunction construction for enhanced visible light-driven photocatalytic activity. *Dalton Trans*. 2019. **48**(10): 3486.
3. Zhong R., Zhang Z., Luo S., Zhang Z.C., Huang L., Gu M. Comparison TiO_2 and g-C_3N_4 2D/2D nanocomposites from three synthesis protocols for visible-light induced hydrogen evolution. *Catal. Sci. Technol*. 2019. **9**(1): 75.
4. Ovcharov M.L., Shvalagin V.V., Granchak V.M. Photocatalytic reduction of CO_2 on mesoporous TiO_2 modified with Ag/Cu bimetallic nanostructures. *Theor. Exp. Chem*. 2014. **50**(3): 175.
5. Stroyuk A.L., Rayevska O.E., Shvalagin V.V., Kuchmiy S.Ya., Bavykin D.V., Streltsov E.A., Poznyak S.K. Gelatin-templated mesoporous titania for photocatalytic air treatment and application in metal-chalcogenide nanoparticle-sensitized solar cells. *Photochem. Photobiol. Sci*. 2013. **12**(4): 621.
6. Liu Q., Tian H., Dai Z., Sun H., Liu J., Ao Z., Wang S., Han C., Liu S. Nitrogen-doped carbon nanospheres-modified graphitic carbon nitride with outstanding photocatalytic activity. *Nano-Micro Lett*. 2020. **12**(1): 1.
7. Wang H., Guan Y., Hu S., Pei Y., Ma W., Fan Z. Hydrothermal synthesis of band gap-tunable oxygen doped g-C_3N_4 with outstanding “two channel” photocatalytic H_2O_2 production ability assisted by dissolution-precipitation process. *Nano*. 2019. **14**(2): 1950023.
8. Jiang T., Liu S., Gao Y., Rony A.H., Fan M., Tan G. Surface modification of porous g-C_3N_4 materials by waste product for enhanced photocatalytic performance under visible light. *Green Chem*. 2019. **21**: 5934.
9. Wen J., Xie J., Chen X., Li X. A review on g-C_3N_4-based photocatalysts. *Appl. Surf. Sci*. 2017. **391**: 72.

10. Qu X., Hu S., Bai J., Li P., Lu G., Kang X. A facile approach to synthesize oxygen doped g-C_3N_4 with enhanced visible light activity under anoxic conditions via oxygen-plasma treatment. *New J. Chem*. 2018. **42**(7): 4998.
11. Liu X., Ji H., Wang J., Xiao J., Yuan H., Xiao D. Ozone treatment of graphitic carbon nitride with enhanced photocatalytic activity under visible light irradiation. *J. Colloid Interface Sci.* 2017. **505**: 919.
12. Wei F., Liu Y., Zhao H., Ren X., Liu J., Hasan T., Chen L., Li Y., Su B. Oxygen self-doped g-C_3N_4 with tunable electronic band structure for unprecedentedly enhanced photocatalytic performance. *Nanoscale*. 2018. **10**(9): 4515.
13. Li J., Shen B., Hong Z. A facile approach to synthesize novel oxygen-doped g-C_3N_4 with superior visible-light photoreactivity. *Chem. Commun*. 2012. **48**(98): 12017.
14. Ming L., Yue H., Xu L., Chen F. Hydrothermal synthesis of oxidized g-C_3N_4 and its regulation of photocatalytic activity. *J. Mater. Chem. A.* 2014. **2**(45): 19145.
15. Yang L.Q., Huang J.F., Shi L., Cao L.Y., Yu Q., Jie Y.N., Fei J., Ouyang H.B., Ye J.H. A surface modification resultant thermally oxidized porous g-C_3N_4 with enhanced photocatalytic hydrogen production. *Appl. Catal. B.* 2017. **204**: 335.
16. Qiu P.X., Xu C.M., Chen H., Fang J., Xin W., Ruifeng L., Xirui Z. One step synthesis of oxygen doped porous graphitic carbon nitride with remarkable improvement of photo-oxidation activity: Role of oxygen on visible light photocatalytic activity. *Appl. Catal. B*. 2017. **206**: 319.
17. Kharlamov A.I., Kharlamova G.A., Bondarenko M.E. New products of a new method for pyrolysis of pyridine. *Russ. J. Appl. Chem*. 2013. **86**(2): 167.
18. Kharlamov O., Bondarenko M., Kharlamova G. O-Doped Carbon Nitride (O-g-C_3N) With High Oxygen Content (11.1 mass %) Synthesized by Pyrolysis of Pyridine. In: *Nanotechnology to Aid Chemical and Biological Defense*, *NATO Science for Peace and Security Series A: Chemistry and Biology*. V. 9. (Dordrecht: Springer Science+Business Media, 2015). P. 129.
19. Kharlamov A.I., Bondarenko M.E., Kharlamova G.A. New method for synthesis of oxygen-doped graphite-like carbon nitride from pyridine. *Russ. J. Appl. Chem.* 2014. **87**(9): 1284.
20. Kharlamov A., Bondarenko M., Kharlamova G. Method for the synthesis of water-soluble oxide of graphite-like carbon nitride. *Diamond Relat. Mater*. 2016. **61**: 46.
21. Kharlamov A., Bondarenko M., Kharlamova G., Gubareni N. Features of the synthesis of carbon nitride oxide (g-C_3N_4)O at urea pyrolysis. *Diamond Relat. Mater*. 2016. **66**: 16.
22. Kharlamov A., Bondarenko M., Kharlamova G., Fomenko V. Synthesis of reduced carbon nitride at the reduction by hydroquinone of water-soluble carbon nitride oxide (g-C_3N_4)O. *J. Solid State Chem*. 2016. **241**: 115.
23. Kharlamov O., Bondarenko M., Kharlamova G., Silenko P., Khyzhun O., Gubareni N. Carbon Nitride Oxide (g-C_3N_4)O and Heteroatomic N-graphene (Azagraphene) as Perspective New Materials in CBRN defense. In: *Nanostructured Materials for the Detection of CBRN, NATO Science for Peace and Security Series A: Chemistry and Biology.* (Springer, Dordrecht, Chapter, V. 20. 2018). P. 245.
24. Bondarenko M., Silenko P., Gubareni N., Khyzhun O., Ostapovskaya N., Solonin Yu. Synthesis of multilayer azagraphene and carbon nitride oxide. *Him. Fiz. Tehnol. Poverhni.* 2018. **9**(4): 393.
25. Bondarenko M., Silenko P., Solonin Yu., Gubareni N., Khyzhun O., Ostapovskaya N. Synthesis O-g-C_3N_4/TiO_2 rutile composite material for photocatalytic application. *Him. Fiz. Tehnol. Poverhni.* 2019. **10**(4): 398.
26. Li H., Wu X., Yin S., Katsumata K., Wang Y. Effect of rutile TiO_2 on the photocatalytic performance of g-C_3N_4/brookite-$TiO_{2-x}N_y$ photocatalyst for NO decomposition. *Appl. Surf. Sci*. 2017. **392**: 531.
27. Li Y., Lv K., Ho W., Dong F., Wu X., Xia Y. Hybridization of rutile TiO_2 (rTiO_2) with g-C_3N_4 quantum dots (CN QDs): An efficient visible-light-driven Z-scheme hybridized photocatalyst. *Appl. Catal. B*. 2017. **202**: 611.
28. Liu C., Wang F., Zhang J., Wang K., Qiu Y., Liang Q., Chen Z. Efficient Photoelectrochemical Water Splitting by g-C_3N_4/TiO_2 Nanotube Array Heterostructures. *Nano-Micro Lett*. 2018. **10**: 37.
29. Xu J., Li Y., Zhou X., Li Y., Gao Z.-D., Song Y.-Y., Schmuki P. Graphitic C_3N_4 sensitized TiO_2 nanotube layers: a visible light activated efficient antimicrobial platform. *Chem. Eur. J*. 2016. **22**(12): 3947.
30. Shalom M., Gimenez S., Schipper F., Herraiz-Cardona I., Bisquert J., Antonietti M. Controlled carbon nitride growth on surfaces for hydrogen evolution electrodes. *Angew. Chem*. 2014. **53**(14): 3654.
31. Boonprakob N, Wetchakun N, Phanichphant S, Waxler D, Sherrell P, Nattestad A, Chen J, Inceesungvorn B. Enhanced visible-light photocatalytic activity of g-C_3N_4/TiO_2 films. *J. Colloid Interface Sci*. 2014. **1**(417): 402.
32. Ren B, Wang T, Qu G, Deng F, Liang D, Yang W, Liu M. In situ synthesis of g-C_3N_4/TiO_2 heterojunction nanocomposites as a highly active photocatalyst for the degradation of Orange II under visible light irradiation. *Environ. Sci. Pollut. Res. Int.* 2018. **25**(19): 19122.
33. Wang P., Guo X., Rao L., Wang C., Guo Y., Zhang L. A weak-light-responsive TiO_2/g-C_3N_4 composite film: photocatalytic activity under low-intensity light irradiation. *Environ Sci. Pollut. Res. Int.* 2018. **25**(20): 20206.

34. Kelyp O.O., Petrik I.S., Vorobets V.S., Smirnova N.P., Kolbasov G.Ya. Sol-gel synthesis and characterization of mesoporous TiO_2 modified with transition metal ions (Co, Ni, Mn, Cu). *Him. Fiz. Tehnol. Poverhni.* 2013. **4**(1): 105.
35. Chubenko E.B., Denisov N.M., Baglov A.V., Bondarenko V.P., Borisenko V.E. Recovery behavior of the luminescence peak from graphitic carbon nitride as a function of the synthesis temperature. *Cryst. Res. Technol*. 2020. **55**(3): 1900163.
36. Liu S., Li D., Sun H. Ang H.M., Tade M.O., Wang S. Oxygen functional groups in graphitic carbon nitride for enhanced photocatalysis. *J. Colloid Interface Sci*. 2016. **468**: 176.
37. Wang C., Fan H., Ren X., Ma J., Fang J., Wang W. Hydrothermally induced oxygen doping of graphitic carbon nitride with a highly ordered architecture and enhanced photocatalytic activity. *Chem. Sus. Chem*. 2018. **11**(4): 700.
38. Pankivska Yu.B., Biliavska L.O., Povnitsa O.Yu., Zagornyi M.M., Ragulia A.V., Kharchuk M.S., Zagorodnya S.D. Antiadenoviral activity of titanium dioxide nanoparticles. *Mikrobiolohichnyi Zhurnal.* 2019. **81**(5): 73.
39. Huang Z.F., Song J., Pan L., Wang Z., Zhang X., Zou J.J. Carbon nitride with simultaneous porous network and O-doping for efficient solar-energy-driven hydrogen evolution. *Nano Energy*. 2015. **12**: 646.
40. Xue J., Fujitsuka M., Majima T. The role of nitrogen defects in graphitic carbon nitride for visible-light-driven hydrogen evolution. *Phys. Chem. Chem. Phys*. 2019. **21**(5): 2318.

Received 31.08.2020, accepted 25.11.2020